Journal of Power Sources 269 (2014) 244–249

Contents lists available at ScienceDirect

Journal of Power Sources

journal homepage: www.elsevier.com/locate/jpowsour

$SrFe_{0.75}Mo_{0.25}O_{3-\delta}$ impregnated 430L alloys for efficient fuel oxidation in metal supported solid oxide fuel cells

Yucun Zhou, Xie Meng, Chun Yuan, Ting Luo, Xiaofeng Ye, Junliang Li, Shaorong Wang*, Zhongliang Zhan*

CAS Key Laboratory of Materials for Energy Conversion, Shanghai Institute of Ceramics, Chinese Academy of Sciences (SICCAS), 1295 Dingxi Road, Shanghai 200050, PR China

HIGHLIGHTS

- Novel SFMO-430L composite anode is prepared for MS-SOFCs.
- Low polarization resistance of 0.11 Ω cm^2 at 800 °C is obtained.
- Promising power density of 0.81 W cm^{-2} is obtained at 800 °C for the MS-SOFC.

ARTICLE INFO

Article history:
Received 4 April 2014
Received in revised form
16 June 2014
Accepted 17 June 2014
Available online 7 July 2014

Keywords:
Metal-supported solid oxide fuel cell
Impregnation
Anode
Molybdenum doped strontium ferrite

ABSTRACT

Here we report a novel $SrFe_{0.75}Mo_{0.25}O_{3-\delta}$ (SFMO)-430L composite anode for the application in the metal supported solid oxide fuel cells. Such an anode is prepared by coating a thin nano porous and mixed electronic-ionic conducting SFMO layer onto the internal surface of a micron porous 430L alloy backbone. The area specific polarization resistance of the composite anode for hydrogen oxidation can be as low as 0.11 Ω cm^2 at 800 °C. The electronic conductivity of the 430L alloy support is found to be critically important for promoting rapid hydrogen oxidation kinetics and attaining such a low polarization resistance as the fuel cell anode. A metal-supported fuel cell with the SFMO impregnated 430L composite anode exhibits outstanding power densities at 800 °C, *e.g.*, 0.81 W cm^{-2} in hydrogen and 0.31 W cm^{-2} in *iso*-octane. Preliminary results show that the present SFMO-430L composite anode exhibits much higher tolerance for coking formation than the traditional Ni-based anode.

1. Introduction

The solid oxide fuel cell (SOFC) is an electrochemical reactor directly converting fuels into electricity and exhibits attractive advantages over the conventional power generation technologies, including high energy efficiency, low pollution emission and wide fuel flexibility [1]. Currently, the common SOFCs consist of yttrium-stabilized zirconia (YSZ) electrolytes sandwiched between the Ni–YSZ anodes and the strontium lanthanum manganite (LSM) cathodes, mostly in the anode-supported configurations [2,3]. Nevertheless, extensive use of expensive and fragile ceramics in the SOFC architecture results in high materials costs and low mechanic reliability, which have been recognized as the main barriers for widespread implementation of the SOFC technology. The novel metal-supported solid oxide fuel cell (MS-SOFC), where a porous alloy provides the mechanical support for thin functional anode–electrolyte–cathode layers, has gained increasing interest due to additional advantages over the common all-ceramic counterpart – including excellent structural robustness and stability, high tolerance toward rapid thermal cycling, easy stack assembling as well as low materials cost [4]. In particular, well-established joining techniques such as brazing and welding can be used for the MS-SOFC stack sealing that is able to withstand large thermal gradients and therefore allows for rapid start-up, making the metal-supported SOFC technology very competitive in the portable and transportation applications where frequent on–off cycling occurs and quick start-up is expected [5,6].

Despite these potential advantages of the MS-SOFCs as shown above, processing challenges should be addressed, especially the anode issues. Most developers of MS-SOFCs tend to co-fire the Ni-based anodes with the metallic supports at an elevated temperature (normally > 1200 °C) to densify the electrolyte layer. In order

* Corresponding authors. Tel./fax: +86 21 6990 6373.
E-mail addresses: zhouycwf@gmail.com (Y. Zhou), srwang@mail.sic.ac.cn (S. Wang), zzhan@mail.sic.ac.cn (Z. Zhan).

http://dx.doi.org/10.1016/j.jpowsour.2014.06.092
0378-7753/

to prevent the metallic support from serious oxidation, the sintering process should be conducted in the reducing atmosphere. However, the co-firing process in a reducing atmosphere would produce unacceptably large Ni particles with reduced surface areas available for fuel oxidation reactions and thereby decreased the fuel cell power densities [7,8]. Furthermore, metallic inter-diffusion occurring between the alloy substrates and the Ni-based anodes during the high temperature co-firing process and during the long-term operation at relative low temperatures is another problem, which would reduce the anode catalytic activity and alter the structural properties of the metallic substrate as well [9–11]. Introducing a barrier layer of ceria, gadolinium doped ceria or $La_{0.6}Sr_{0.2}Ca_{0.2}CrO_3$ between the metallic support and the anode could prevent such metallic inter-diffusion, but could not address the issue of Ni coarsening during the co-firing process [9,10]. Low temperature thin film deposition techniques, including plasma spray method [12,13], and pulsed laser deposition (PLD) [14] have been used to form the functional ceramic layers on the metallic substrates to avoid excessive Ni coarsening and metallic inter-diffusion but would lead to high manufacturing costs. Alternatively, the anode catalysts could also be introduced into the pre-fired anode porous backbones at relatively low temperatures by the impregnating method [15–17]. Despite these extensive efforts, developing a durable and efficient anode catalyst for the robust metal-supported fuel cell remains a significant challenge.

As reported, $Sr_2Fe_{1.5}Mo_{0.5}O_{6-\delta}$ (SFMO) is a good electrode catalyst due to its good structural stability and important mixed ionic-electronic conducting behavior in both oxidizing and reducing atmospheres [18,19]. Here we report a novel robust, durable anode structure consisting of a nano porous SFMO catalyst coating supported on the internal surfaces of a micron porous 430L alloy backbone that exhibits impressive catalytic activity for fuel oxidation reactions and thereby yields low polarization resistances.

2. Experimental

For symmetrical anode fuel cells, the tri-layer structure of porous 430L|dense YSZ|porous 430L was produced by laminating three tape-cast green tapes, with 30 wt% ammonia oxalate used as the fugitive material for the two porous 430L substrates. The YSZ powders (7 m^2 g^{-1}) were purchased from Tosoh Corporation (Japan), and the 430L stainless steel powers (−400 mesh) were supplied by Jing-Yuan Powder Material (China). The slurry for tape casting was ethanol-based and consisted of acrylic resin dispersants, polyvinyl butyral binders, dibutyl phthalate plasticizer and other organic additives in addition to alloy or ceramic powders. Green tapes were obtained by casting appropriate slurries on the Mylar carrier on the tape casting machine (Lab-Cast Model TC-71LC Tape Caster, HED International, USA). The laminated green tapes were co-fired in a reducing atmosphere of 5% H_2–95% N_2 at 1320 °C to produce the final structures. The SFMO catalysts were added into the porous 430L backbones by impregnating an aqueous solution containing $Sr(NO_3)_2$, $Fe(NO_3)_3{\cdot}9H_2O$, $(NH_4)_6Mo_7O_{24}{\cdot}4H_2O$ and citric acid in a molar ratio of 1:0.75:0.0357:2, followed by calcinations at 850 °C in a reducing atmosphere of 5% H_2–95% N_2 for 2 h to prevent oxidation of the 430L substrate. These salts were 99% pure and purchased from Sinopharm Chemical Reagent. The loadings of impregnated catalysts were controlled by a micro-liter syringe each time and a single impregnation–calcination cycle could yield an infiltrate loading of ≈3 vol%. The ultimate catalyst loadings were tailored by increasing the impregnation–calcination cycles.

For single fuel cells, the tri-layer structure of porous 430L|dense YSZ|porous YSZ was produced by laminating three tape-cast green tapes, followed by co-firing at 1320 °C in 5% H_2–95% N_2 [20]. Impregnation of SFMO catalysts was performed as described above, yielding V_{SFMO} = 16.0% SFMO-430L composite anodes and V_{SFMO} = 32.8% SFMO–YSZ composite cathodes. A single impregnation–calcination cycle could generate an infiltrate loading of ≈6 vol% for the cathode.

The electrochemical properties of the SFMO-430L composite anodes were assessed on both symmetric anode cells and functional metal-supported cells over the temperature range of 650–800 °C. Silver ink was applied on the electrode surface as the current collector, and silver wires were used as the current leads. Current–voltage curves and electrochemical impedance spectra were obtained using an IM6 Electrochemical Workstation (ZAHNER, Germany). The frequency range for impedance measurement was 0.1 Hz–100 kHz with a 20 mV AC amplitude. Humidified (3% H_2O) hydrogen at a flow rate of 100 sccm, mixed with nitrogen in some cases, was used for measurement of the anode polarization resistance in the symmetric cells. The metal-supported fuel cell was tested with dry air at 100 sccm maintained in the cathode. The fuel in the anode was 97% H_2–3% H_2O at 100 sccm or 6% *iso*-octane–94% nitrogen. Active area of the symmetric anode cell and the single cell was 0.64 cm^2 and 0.35 cm^2, respectively.

For electrical conductivities test, SFMO powers were prepared by a combustion synthesis technique that used the corresponding metal nitrates and citric acid as the precursors. The as-synthesized SFMO powders were compacted into a bar and then fired in air at 1350 °C, yielding a relative density of 95% as measured by the

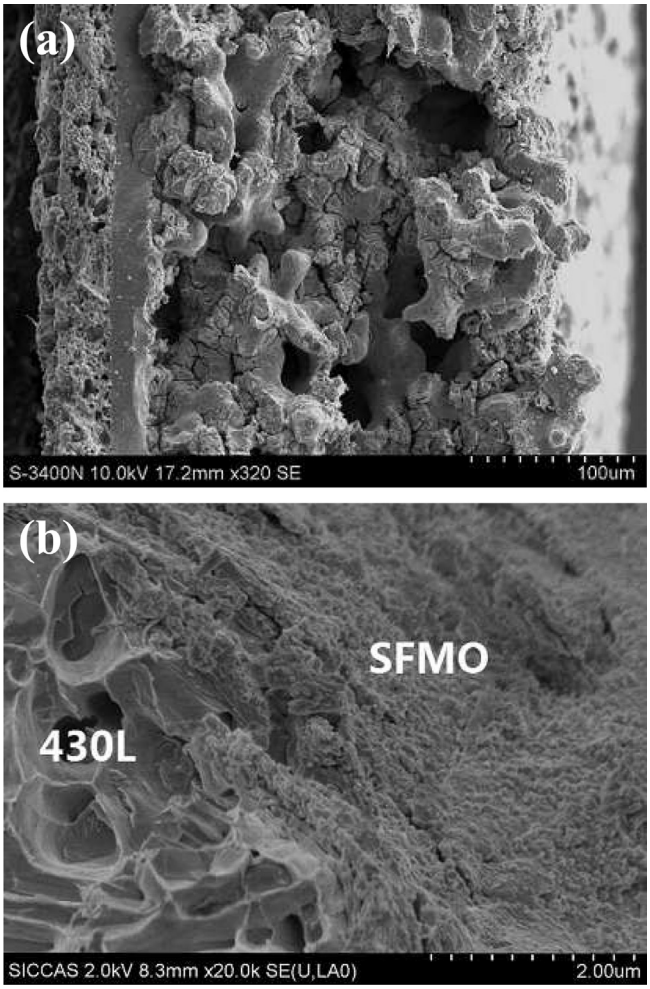

Fig. 1. (a) Cross-sectional scanning electron microscope (SEM) image of the MS-SOFC. (b) A higher magnification SEM image of the impregnated SFMO/430L anode.

Archimedes' method. The electrical conductivities were measured in 97% H_2–3% H_2O by a standard four-probe DC method. The cell structure was examined after testing using scanning electron microscopy (SEM) in a Hitachi S-4800-II microscope. Raman spectrums of cell anodes after operating in hydrogen and *iso*-octane were analyzed by Raman microscope (Renishaw, Invia Raman microscope) with a 514 nm He–Ne laser as the excitation source. The laser spot size is about 1 μm.

3. Results and discussion

Fig. 1(a) shows a cross-sectional SEM micrograph of the single MS-SOFC as prepared, consisting of a porous SFMO impregnated YSZ cathode (Left side, $V_{SFMO} = 32.8\%$), a dense YSZ electrolyte and a porous SFMO impregnated 430L anode substrate (Right side, $V_{SFMO} = 16.0\%$). The thickness of the cell component is about 40 μm, 23 μm and 250 μm for the cathode, electrolyte and anode, respectively. Good bonding between the electrolyte and the adjacent layers is presented clearly. Fig. 1(b) shows an SEM micrograph of the resulting SFMO-430L composite anode at a volume loading of SFMO catalysts (V_{SFMO}) of 16.0% that exhibits a thin porous and well intra-connected SFMO coating on the internal surfaces of the porous 430L backbone. A higher-magnification SEM micrograph of the SFMO coating with an average SFMO particle diameter of ≈60 nm and a pore diameter of ≈40 nm is shown elsewhere [8].

Such a nano-scale structure has substantially larger surface area than the traditional micron-scale anode and therefore allows for fast fuel oxidation kinetics [21,22].

Fig. 2 shows (a) Bode and (b) Nyquist plots of the EIS data for symmetric anode cells at different SFMO loadings, measured in a uniform atmosphere of 97% H_2–3% H_2O at 800 °C, where the pure ohmic resistances due to the electrolyte and the conducting wires were subtracted from the cell impedance while the interfacial polarization resistances were divided by 2 to account for the contribution of two symmetric anodes. Fig. 2(c) summarizes the $R_{P,A}$ values at varied SFMO loadings. Notably, tailoring the SFMO catalyst loading is important to obtain an overall low polarization resistance given that the electrochemical reactions occurring on the SFMO catalysts consist of several consecutive steps, including gas diffusion within the porous backbones, gas adsorption on the SFMO catalyst surfaces, surface diffusion and ionization of adsorbed atoms, ion transport in the bulk SFMO coatings and charge transfer at the SFMO|YSZ interfaces. Increasing the SFMO loadings within the porous backbone produced more surface area available for surface adsorption, but in the meanwhile decreased the porosity of the backbone that would increase the gas diffusion resistance. Balancing such conflicting requirements yielded an optimized SFMO loading of $V_{SFMO} = 16.0\%$ for the SFMO-430L anodes. The optimized SFMO loading of the cathode is also studied elsewhere and the $V_{SFMO} = 32.8\%$ is found to be the best [8].

Fig. 2(a) also shows that impedance spectra consisted of two responses with the relaxation frequencies centered at ≈100 Hz and ≈1 Hz, respectively. In order to gain insights into hydrogen oxidation kinetics over the SFMO impregnated 430L composites, impedance measurements were also performed at varied temperatures and hydrogen partial pressures (P_{H2}) for symmetric anode cells at $V_{SFMO} = 16.0\%$ (Fig. 3), and these impedance data were fitted using the equivalent circuits $L(R^H,C^H)$ (R^L,C^L), where L was the inductance due to connecting wires, R^H and R^L were widths for the higher- and lower-frequency arcs, while C^H and C^L were the constant phase elements for the higher- and lower-frequency arcs.

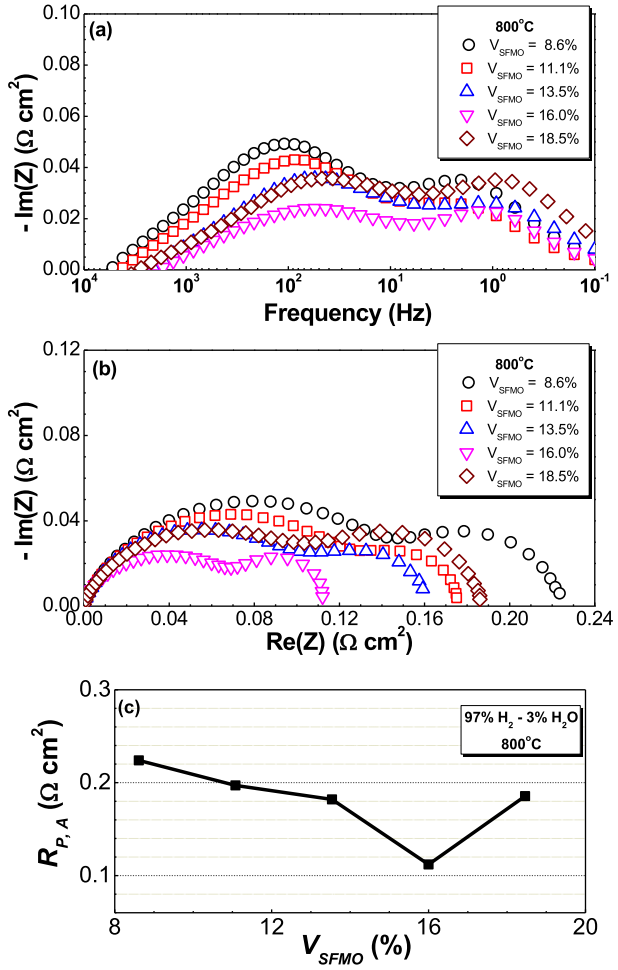

Fig. 2. (a) Bode plots of impedance data measured in 97% H_2–3% H_2O at 800 °C for symmetric anode cells with different SFMO loadings. (b) Nyquist plot of the data shown in (a). (c) The anode polarization resistance (R_P) at 800 °C *versus* the SFMO loading (V_{SFMO}).

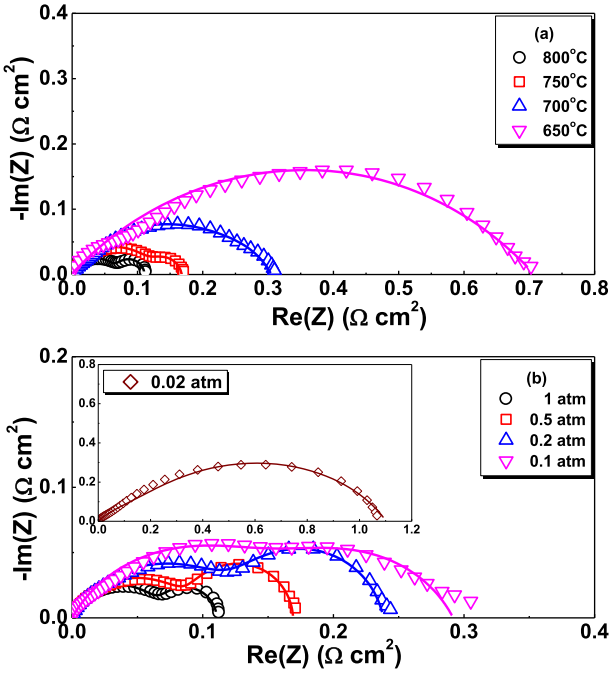

Fig. 3. Impedance data measured for symmetric anode cells at $V_{SFMO} = 16.0\%$: (a) Nyquist plots in 97% H_2–3% H_2O at different temperatures and (b) Nyquist plots at 800 °C in atmospheres with different hydrogen partial pressures. Included were the fitting results based upon the equivalent circuits $L(R^H,Q^H)$ (R^L,Q^L).

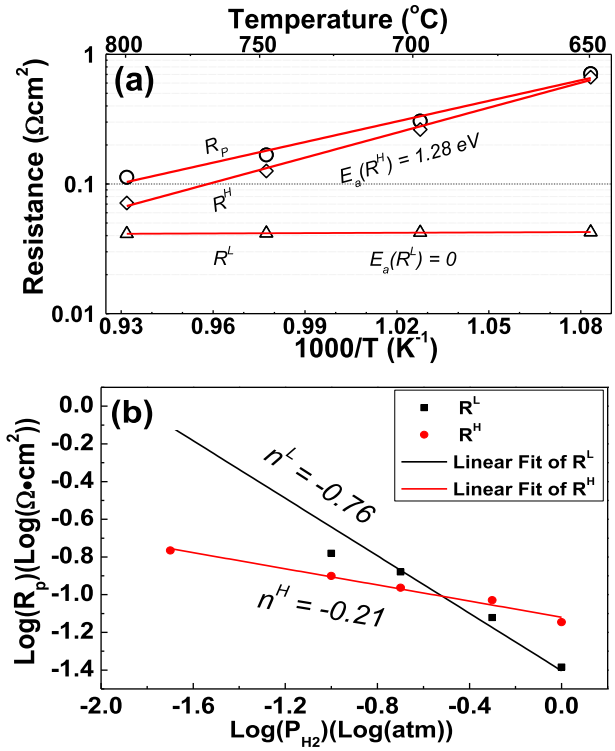

Fig. 4. (a) Temperature dependence of the anode polarization resistance, the higher- and lower-frequency arcs of the impedance data measured for symmetric anode cells. (b) Hydrogen partial pressure dependence of the higher- and lower-frequency arcs of the impedance data.

Summarized in Fig. 4(a) are the R^H, R^L and R_P (Anode polarization resistance) values at varied temperatures for the V_{SFMO} = 16.0% SFMO-430L composite in 97% H_2–3% H_2O. Notably, the R_P values increase from 0.11 Ω cm^2 at 800 °C to 0.70 Ω cm^2 at 650 °C. Those results are impressively low especially given that SFMO catalysts are coated on the internal surfaces of electronic conducting 430L alloys that do not allow for oxide ionic conduction. As a matter of fact, the electronic conductivity of the supporting component critically influences the catalytic and electrochemical behavior of the dual-scale composite anodes since the total conductivity of SFMO catalyst is relatively low in the reducing atmosphere when compared to the common Ni–cermet anode (Fig. 5). For comparison, the SFMO impregnated $La_{0.9}Sr_{0.1}Ga_{0.8}Mg_{0.2}O_{3-\delta}$ (LSGM) composite was fabricated based upon a porous|dense|porous LSGM tri-layer structure, where the pure oxide-ion conducting ceramics was used as the porous backbone. Impedance measurement in 97% H_2–3% H_2O indicated that the polarization resistance for the SFMO–LSGM composite was 0.25 Ω cm^2 at 750 °C [23], which is lager than the result of 0.17 Ω cm^2 as obtained here. Additional, the impregnated SFMO-430L composite anodes also show substantially smaller polarization resistances than prior alternative oxide anodes, *e.g.*, 0.43 Ω cm^2 for $Mn_{1.5}Co_{1.5}O_4$ impregnated YSZ anodes [24] and 0.21 Ω cm^2 for $La_{0.6}Sr_{0.4}Fe_{0.9}Sc_{0.1}O_{3-\delta}$ impregnated 430L anodes measured at 800 °C [25], 5.1 Ω cm^2 for CeO_2 impregnated FeCr alloy-YSZ cermets and 1.2 Ω cm^2 for $Ce_{0.8}Gd_{0.2}O_{2-\delta}$ (GDC) impregnated FeCr alloy-YSZ cermets measured at 650 °C [26]. Therefore, the superior catalytic activity of the present SFMO-430L composite for hydrogen oxidation reactions can be explained by the facilitated mixed oxide ionic

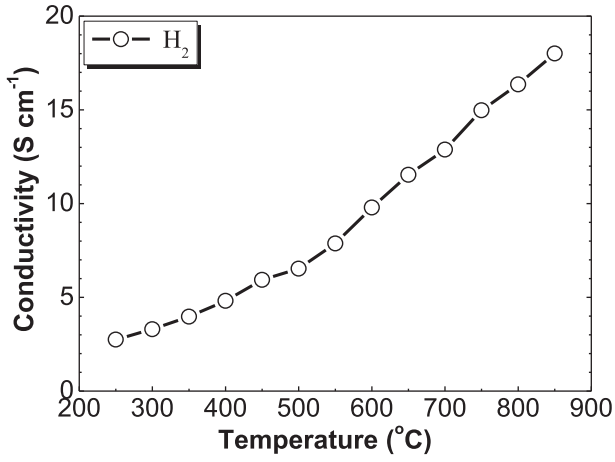

Fig. 5. Electrical conductivities of the SFMO catalysts measured at different temperatures in hydrogen.

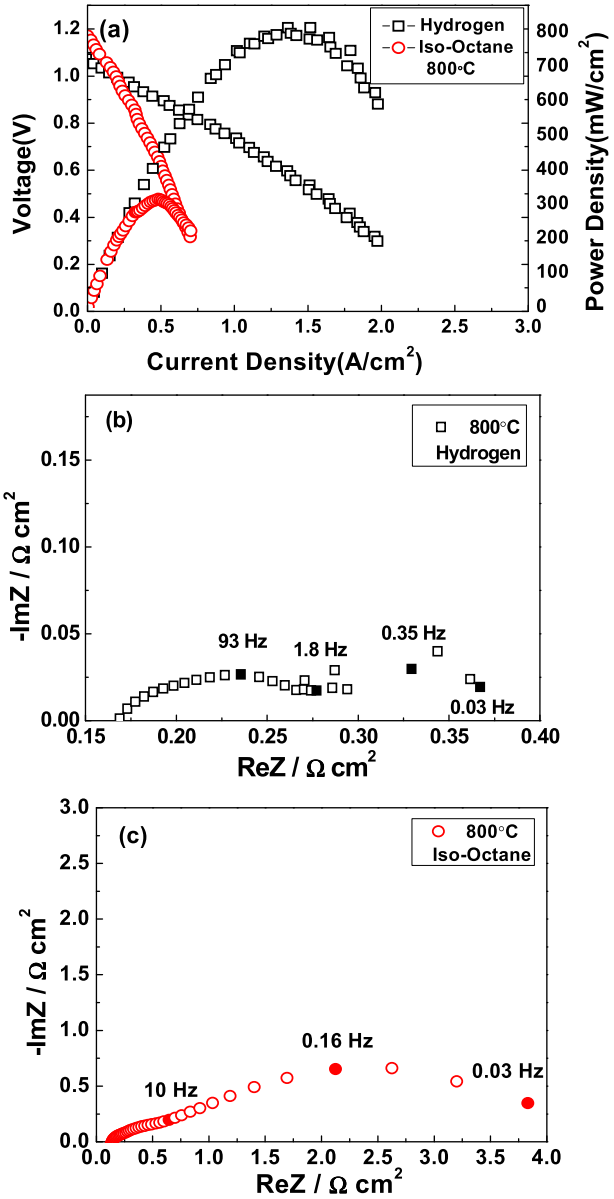

Fig. 6. (a) Voltage and power density *versus* current density for the present MS-SOFC operating in hydrogen and *iso*-octane. (b) Nyquist plots of the impedance data for the cell operating in hydrogen. (c) Nyquist plots of the impedance data for the cell operating in *iso*-octane.

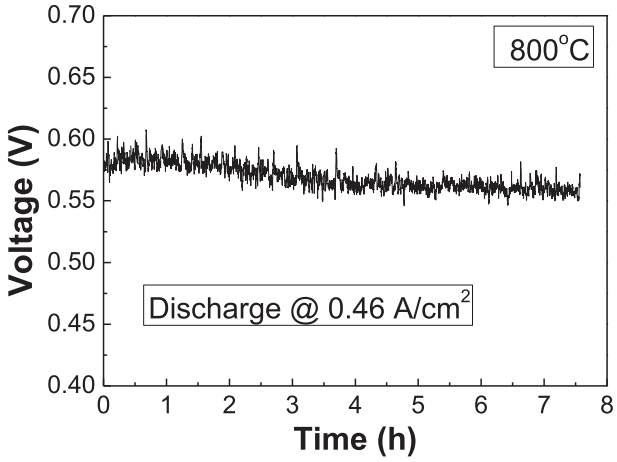

Fig. 7. Short-term stability of the MS-SOFC with *iso*-octane fuel.

and electronic conducting behavior of SFMO catalysts [19,27,28], enlarged surface area of the nano porous SFMO coatings, and the sufficient electronic conductivities of the 430L supports as well.

Fig. 4(a) also shows that the R^H value followed Arrhenius dependence over the temperature regime of 650–800 °C while the R^L value remained almost unchanged with temperature. The activation energy for the higher-frequency arc was 1.28 eV. These results seemingly suggest that the higher-frequency arc might be correlated with the charge transfer reaction on the SFMO|YSZ interfaces, and that the lower-frequency arc is likely related to the hydrogen surface adsorption process [29,30]. This conclusion is further supported by the observation that the lower-frequency arc increased substantially with decreasing hydrogen partial pressure, while the higher-frequency arc changed little with hydrogen partial pressure (Fig. 4(b)). Furthermore, linear fitting between Log(R_P) and Log(P_{H2}) yields a slope of 0.76 and 0.21 for the lower-frequency arc and the higher-frequency arc, respectively. It indicates that non-dissociative adsorption of hydrogen might dominate the SFMO surfaces and become the rate-limiting step at low hydrogen partial pressures.

Fig. 6(a) shows the cell voltages (V) and power densities (P) as a function of current densities (J) for the single fuel cell with the structure of SFMO impregnated 430L anode|YSZ electrolyte|SFMO impregnated YSZ cathode. The measurement was conducted at 800 °C with 97% H_2–3% H_2O fuels and dry air oxidants at 100 sccm in the anode and cathode, respectively. As shown in Fig. 6(a), the maximum power density of the fuel cell is 0.81 W cm^{-2}. The present MS-SOFC compares favorably with prior metal-supported fuel cells in terms of power density, technical viability and fabrication simplicity. For example, MS-SOFC with the same structure and impregnated LSFSc electrodes showed a relatively low maximum power density of 0.65 W cm^{-2} at 800 °C [25]. Metal-supported fuel cells obtained using the plasma spray technique to deposit the functional SOFC layers as well as the diffusion barrier layer exhibited power densities of 0.61 W cm^{-2} at 800 °C [31]. Tucker et al. demonstrated initial power densities of ≈0.35 W cm^{-2} at 700 °C for MS-SOFC with impregnated Ni anodes and LSM cathodes [15]. Despite there are reports on high power densities for MS-SOFCs, those performances are obtained with more conductive and thinner electrolytes and with Ni contain anode that commonly showed much higher catalytic activity for hydrogen oxidation reactions than the present SFMO oxide anode [12,16,32].

Note that the oxide anode like SFMO, when exposed to hydrocarbon fuels, typically exhibits higher tolerance toward coking formation than the standard Ni–cermet anode [33,34]. Fig. 6(a) shows the performance of the present metal-supported fuel cells with SFMO impregnated 430L anodes operating on the *iso*-octane fuels, yielding a maximum power density of 0.31 W cm^{-2} at 800 °C. The performance is comparable with that previous reported for the $La_{0.9}Sr_{0.1}Ga_{0.8}Mg_{0.2}O_{3-\delta}$ (LSGM)-electrolyte based SOFC with the SFMO impregnated LSGM anode [23]. A comparison of the resistances for the fuel cell with hydrogen and *iso*-octane as fuels is

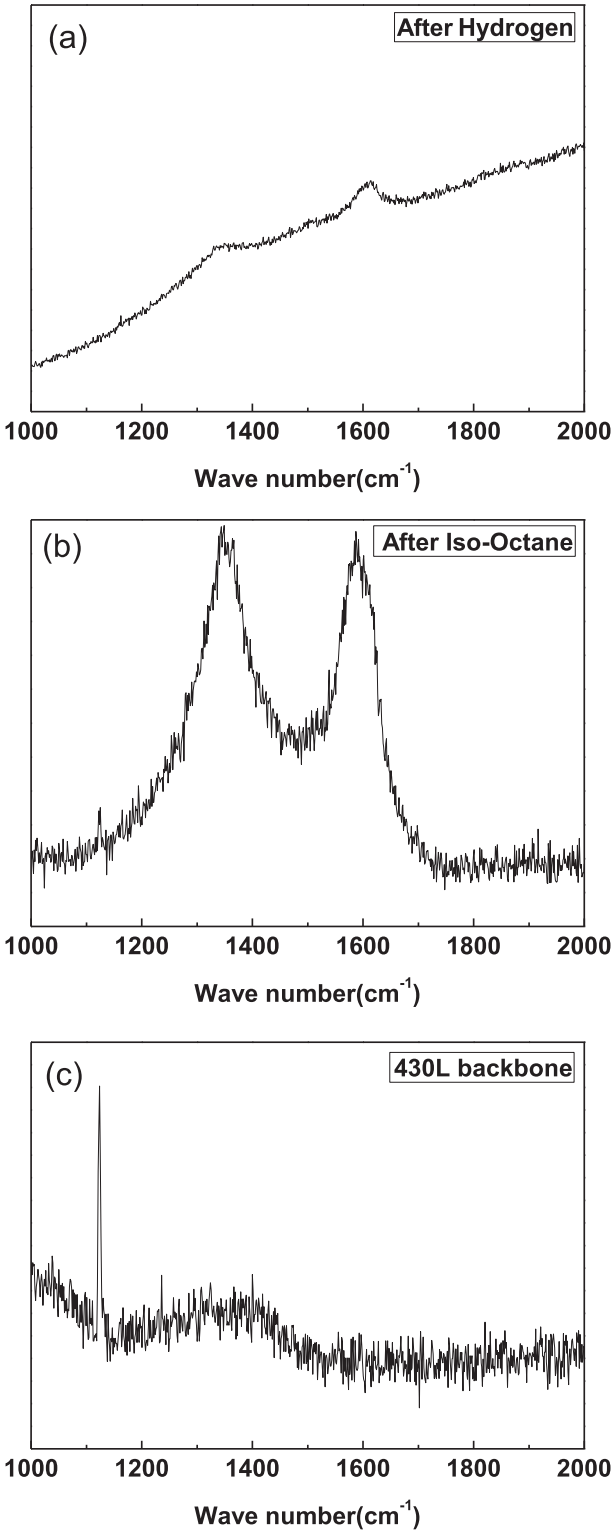

Fig. 8. (a) Raman spectra of the cell anode after operating in hydrogen. (b) Raman spectra of the cell anode after operating in *iso*-octane. (c) Raman spectra of the 430L backbone before impregnation.

shown in Fig. 6(b) and (c). The pure ohmic loss shows no obvious difference, while the polarization loss is quite different and an enlarged low-frequency arc centered at 0.16 Hz is shown for the cell with *iso*-octane fuel. The difference of the polarization loss for the same cell with different fuels may be caused by the variation of the activation and diffusion processes in the anode.

In order to examine the short-term stability of the fuel cell with *iso*-octane fuel, the present MS-SOFC was operated for 7.5 h under a constant current density of 0.46 A cm^{-2} at 800 °C. Fig. 7 shows that the cell voltage decreased continuously from approximately 0.58 V–0.56 V when operated in *iso*-octane. Since Raman spectroscopy has been demonstrated to be an effective tool for investigating coking on the SOFC anodes operating under carbon-containing fuels [35], the Raman spectra of cell anodes after operating in hydrogen and *iso*-octane are collected and shown in Fig. 8. Note that even operating in hydrogen atmosphere, the peak at around 1350 cm^{-1} and 1580 cm^{-1} which assigned to the popularly known D and G bands is observed (Fig. 8(a)), such Raman peak composed of the D and G components is one of the most widely investigated attributes in amorphous carbon films [36,37]. Since the SFMO catalysts were introduced into the cell anodes by calcining the impregnation solution containing citric acid at 850 °C in a reducing atmosphere, the amorphous carbon observed may be caused by the incomplete combustion of citric acid. The conclusion is further supported by the Raman spectra of the 430L backbone before impregnation. As shown in Fig. 8(c), no typical carbon peak is observed for the blank 430L backbone. For the cell anode after operating in *iso*-octane, the Raman peak of amorphous carbon is very obvious (Fig. 8(b)). We surmise that the carbon deposition in the cell anode may be the main reason for the performance degradation of the single cell as shown in Fig. 7(a). Although extended tests are required for better evaluation of the long-term stability and carbon deposition issue, preliminary results show that the present SFMO-430L composite anode exhibits much higher tolerance for coking formation than the traditional Ni-based anode [38,39].

4. Conclusions

In summary, we have fabricated a novel composite anode of SFMO-430L by coating a thin nano porous and mixed electronic-ionic conducting SFMO layer onto the internal surface of a micron porous and pure electronic conducting 430L alloy backbone. The area specific polarization resistance of the composite as the fuel cell anode for hydrogen oxidation can be as low as 0.11 Ω cm^2 at 800 °C. We further showed that the electronic conductivity of the 430L alloy support is critically important for promoting rapid hydrogen oxidation kinetics and attaining such a low polarization resistance as the fuel cell anode. We also demonstrated that a metal-supported fuel cell with the SFMO impregnated 430L composite anode exhibited outstanding power densities at 800 °C, *e.g.*, 0.81 W cm^{-2} in hydrogen and 0.31 W cm^{-2} in *iso*-octane. Even though carbon deposition in the cell anode after operating in *iso*-octane is detected, the potential tolerance ability toward coking formation is exhibited for the SFMO-430L anode.

Acknowledgment

We gratefully acknowledge the financial support from the Chinese Government High Tech Developing Project (2011AA050702), National Basic Research Program of China (No. 2012CB215400) and National Natural Science Foundation of China (No. 51172266).

References

[1] N.Q. Minh, Solid State Ionics 174 (2004) 271–277.
[2] R.M. Ormerod, Chem. Soc. Rev. 32 (2003) 17–28.
[3] A.J. Jacobson, Chem. Mater. 22 (2009) 660–674.
[4] M.C. Tucker, J. Power Sources 195 (2010) 4570–4582.
[5] M.C. Tucker, C.P. Jacobson, L.C. De Jonghe, S.J. Visco, J. Power Sources 160 (2006) 1049–1057.
[6] Y.B. Matus, L.C. De Jonghe, C.P. Jacobson, S.J. Visco, Solid State Ionics 176 (2005) 443–449.
[7] I. Villarreal, C. Jacobson, A. Leming, Y. Matus, S. Visco, L. De Jonghe, Electrochem. Solid State Lett. 6 (2003) A178–A179.
[8] Y. Zhou, X. Meng, X. Ye, J. Li, S. Wang, Z. Zhan, J. Power Sources 247 (2014) 556–561.
[9] T. Franco, K. Schibinger, Z. Ilhan, G. Schiller, A. Venskutonis, Ceramic diffusion barrier layers for metal supported SOFCs, in: K. Eguchi, S.C. Singhai, H. Yokokawa, H. Mizusaki (Eds.), Solid Oxide Fuel Cells, vol. 10, 2007, pp. 771–780.
[10] M. Brandner, M. Bram, J. Froitzheim, H.P. Buchkremer, D. Stoever, Solid State Ionics 179 (2008) 1501–1504.
[11] J.H. Choi, T. Lee, M. Choi, Y.-S. Yoo, S.-W. Baek, J. Bae, Int. J. Hydrogen Energy 35 (2010) 4285–4291.
[12] C.-S. Hwang, C.-H. Tsai, J.-F. Yu, C.-L. Chang, J.-M. Lin, Y.-H. Shiu, S.-W. Cheng, J. Power Sources 196 (2011) 1932–1939.
[13] R. Vassen, D. Hathiramani, J. Mertens, V.A.C. Haanappel, I.C. Vinke, Surf. Coat. Technol. 202 (2007) 499–508.
[14] Y.-W. Ju, T. Inagaki, S. Ida, T. Ishihara, J. Electrochem. Soc. 158 (2011) B825–B830.
[15] M.C. Tucker, G.Y. Lau, C.P. Jacobson, L.C. DeJonghe, S.J. Visco, J. Power Sources 171 (2007) 477–482.
[16] T. Klemenso, J. Nielsen, P. Blennow, A.H. Persson, T. Stegk, B.H. Christensen, S. Sonderby, J. Power Sources 196 (2011) 9459–9466.
[17] Z. Liu, B. Liu, D. Ding, Z. Jiang, C. Xia, Int. J. Hydrogen Energy 37 (2012) 4401–4405.
[18] Q. Liu, X. Dong, G. Xiao, F. Zhao, F. Chen, Adv. Mater. 22 (2010) 5478–5482.
[19] A.B. Muñoz-García, D.E. Bugaris, M. Pavone, J.P. Hodges, A. Huq, F. Chen, H.-C. zur Loye, E.A. Carter, J. Am. Chem. Soc. 134 (2012) 6826–6833.
[20] Y. Zhou, X. Ye, J. Li, Z. Zhan, S. Wang, J. Electrochem. Soc. 161 (2014) F332–F336.
[21] Z. Zhan, D.M. Bierschenk, J.S. Cronin, S.A. Barnett, Energy Environ. Sci. 4 (2011) 3951–3954.
[22] Z. Zhan, D. Han, T. Wu, X. Ye, S. Wang, T. Wen, S. Cho, S.A. Barnett, RSC Adv. 2 (2012) 4075–4078.
[23] X. Meng, X. Liu, D. Han, H. Wu, J. Li, Z. Zhan, J. Power Sources 252 (2014) 58–63.
[24] X. Liu, D. Han, H. Wu, X. Meng, F. Zeng, Z. Zhan, Int. J. Hydrogen Energy 38 (2013) 16563–16568.
[25] Y. Zhou, X. Liu, J. Li, H. Nie, X. Ye, S. Wang, Z. Zhan, J. Power Sources 252 (2014) 164–168.
[26] P. Blennow, J. Hjelm, T. Klemenso, A.H. Persson, S. Ramousse, M. Mogensen, Fuel Cells 11 (2011) 661–668.
[27] A.B. Munñoz-García, M. Pavone, E.A. Carter, Chem. Mater. 23 (2011) 4525–4536.
[28] A.B. Muñoz-García, M. Pavone, A.M. Ritzmann, E.A. Carter, Phys. Chem. Chem. Phys. 15 (2013) 6250–6259.
[29] S. Jiang, S. Badwal, Solid State Ionics 123 (1999) 209–224.
[30] M. Chen, B.H. Kim, Q. Xu, B.G. Ahn, D.P. Huang, Solid State Ionics 181 (2010) 1119–1124.
[31] A. Ansar, P. Szabo, J. Arnold, Z. Ilhan, D. Soysal, R. Costa, A. Zagst, M. Gindrat, T. Franco, Metal supported solid oxide fuel cells and stacks for auxiliary power units – progress, challenges and lessons learned, in: S.C. Singhal, K. Eguchi (Eds.), Solid Oxide Fuel Cells, vol. 12, 2011, pp. 147–155.
[32] Y.-W. Ju, S. Ida, T. Ishihara, RSC Adv. 3 (2013) 10508–10515.
[33] H. Li, Y. Tian, Z. Wang, F. Qie, Y. Li, RSC Adv. 2 (2012) 3857–3863.
[34] Q. Liu, D.E. Bugaris, G. Xiao, M. Chmara, S. Ma, H.-C. zur Loye, M.D. Amiridis, F. Chen, J. Power Sources 196 (2011) 9148–9153.
[35] K.S. Blinn, H. Abernathy, X. Li, M. Liu, L.A. Bottomley, M. Liu, Energy Environ. Sci. 5 (2012) 7913–7917.
[36] P.K. Chu, L. Li, Mater. Chem. Phys. 96 (2006) 253–277.
[37] A. Ferrari, J. Robertson, Phys. Rev. B 64 (2001) 075414.
[38] Z.L. Zhan, S.A. Barnett, Science 308 (2005) 844–847.
[39] G. Xiao, F. Chen, Electrochem. Commun. 13 (2011) 57–59.